Title

The Transport of Asian Dust and Combustion Aerosols and Associated Ozone to North America as Observed From a Mountaintop Monitoring Site in the California Coast Range

Journal

Journal of Geophysical Research: Atmospheres, 123(10)

ISSN

2169-897X

Authors

Asher, Elizabeth C
Christensen, John N
Post, Andrew
et al.

Publication Date

2018-05-27

DOI

10.1029/2017jd028075

Peer reviewed

The Transport of Asian Dust and Combustion Aerosols and Associated Ozone to North America as Observed From a Mountaintop Monitoring Site in the California Coast Range

Elizabeth C. Asher[1,2], John N. Christensen[3], Andrew Post[1,4], Kevin Perry[5], Steven S. Cliff[6], Yongjing Zhao[6], Justin Trousdell[1], and Ian Faloona[1]

1 Department of Land Air and Water Resources, University of California, Davis, CA, USA,

2 Now at the National Center for Atmospheric Research, Boulder, CO, USA,

3 Lawrence Berkeley National Laboratory, Berkeley, CA, USA,

4 Now at California Air Resources Board, Sacramento, CA, USA,

5 Atmospheric Sciences, University of Utah, Salt Lake City, UT, USA,

6 Air Quality Research Center, University of California, Davis, CA, USA

Correspondence to: I. Faloona, icfaloona@ucdavis.edu

Abstract

Aerosol and tropospheric ozone transport to North America has important implications for regional air quality and climate. We present data from Chews Ridge, a remote mountaintop site in California, in February–September 2012, which identifies separate Asian dust and Asian combustion aerosol signals and quantifies exogenous ozone. We use positive matrix factorization of size-fractionated aerosol X-ray fluorescence data and $^{206}Pb/^{207}Pb$ and $^{208}Pb/^{207}Pb$ isotope measurements to isolate aerosol signals of Asian origins and find good agreement between both types source attribution techniques. Power spectra of Asian dust and Asian combustion signals reveal two distinct peaks, one seasonal (~90 days) and one monthly (~25–30 days). Overall, 89% of the Asian dust signal occurs in March–May, compared with June–September, whereas only 51% of the Asian combustion signal occurs in March–May. Nearly half the Pb observed at Chews Ridge was derived from Asia (46%; 8.3% from Asian dust, 23% from Asian combustion, and 15% of the Asian Pb signal was not explained by the positive matrix factorization). A positive correlation between deseasonalized ozone concentrations and the Asian factors suggests that ozone is elevated by 6.3 ± 0.8 ppb due to transpacific transport. Scanning mobility particle size spectra were also measured from May to September and indicate that new particles are often produced and grow throughout the afternoon during onshore flow. We hypothesize that particle nucleation on the windward edge of the continent is an important source of new particles.

1 Introduction

Aerosols are solid or liquid particles suspended and transported in the atmosphere, which can either scatter or absorb solar and infrared radiation based on aerosol composition and light wavelength. Numerous factors dictate the specific climate and hydrologic impacts of aerosol-cloud and aerosol-radiation interactions: aerosol composition, size, atmospheric

lifetime, altitude, and geographic location (Intergovernmental Panel on Climate Change, 2014). Aerosols are either lofted into the atmosphere (i.e., sea salt spray, dust, or pollen) or formed in clean air masses through heterogeneous chemical reactions (Pöschl, 2005). These small particles can appreciably alter the Earth's albedo and influence precipitation patterns by acting as efficient cloud-condensing nuclei (e.g., McCoy et al., 2015; Rosenfeld et al., 2008). Aerosols may continue to influence Earth's albedo, radiative heating, and the hydrologic cycle following their dry deposition on snow-covered surfaces (Hadley et al., 2010).

High concentrations of fine aerosols (aerodynamic diameter ≤ 2.5 μm, particulate matter 2.5, PM2.5) also adversely affect air quality and human health (World Health Organization, 2013). The Environmental Protection Agency (EPA) has sought to regulate concentrations of PM2.5 by mass since 1997 in the United States, most recently setting a maximum 24-hr attainment standard of 35 $\mu g/m^3$ in 2006 and a yearly mean attainment standard of 12 $\mu g/m^3$ in 2012 Table of Historical Ozone National Ambient Air Quality Standards, 2018; Table of Historical Particulate Matter (PM) National Ambient Air Quality Standards, 2018. In contrast, particulate pollution in Chinese cities often surpasses their local 24-hr attainment standard of 75 $\mu g/m^3$, reaching concentrations >300 $\mu g/m^3$ largely due to secondary aerosol contributions (e.g., Huang et al., 2014). The long-range transport of anthropogenic aerosols and pollutants has received considerable attention as a source for particulate pollution due to the growing disparity between North American and Asian air quality. An estimated ~6,600 premature deaths occurred in 2000 in North America as a direct result of foreign (transported) PM2.5 (Liu et al., 2009).

Using data from the Moderate Resolution Imaging Spectroradiometer (MODIS) and the Cloud-Aerosol Lidar with Orthogonal Polarization (CALIOP), Yu et al. (2012) have argued that the transcontinental transport of dust and to a lesser extent small combustion aerosols from Asia, Africa, and Europe outweigh that of locally produced combustion aerosols over North America. Field campaigns conducted in March–May at Mt. Bachelor, Oregon (2,763 m), and Whistler Peak, British Columbia (2,184 m), present evidence that free tropospheric air masses (~2–6 km altitude) carry dust and secondary sulfate aerosols to the west coast of North America (Fischer et al., 2011; Leaitch et al., 2009; McKendry et al., 2008). Asian dust and biomass burning plumes are depleted in fine organic aerosol, compared with local air masses (Brock et al., 2004; Sun et al., 2009). Indeed, several recent studies indicate that transcontinental transport leads to elevated plumes of dust and pollutants in the western United States, while organic aerosol is produced locally and largely remains trapped in the boundary layer (e.g., Hu et al., 2016; Lin et al., 2012). Airborne observations off the west coast of California and Oregon (Brock et al., 2004) show that air masses advected across the Pacific may maintain distinct plumes of coarse mode dust particles, biomass burning plumes, and secondary sulfate aerosol (Lin et al., 2012). Additional ground-

based mountaintop observations could help determine the frequency, net impact, and regional and seasonal variability in transpacific transport of aerosols and pollutants to the west coast of North America.

Since the 1980s the transpacific transport of Asian dust has been widely recognized as an important source of nutrients to the iron-limited Northeast Pacific Ocean and the dominant spring signal in the aerosol record at remote monitoring sites in the Western United States (Duce et al., 1980; Holmes & Zoller, 1996; Martin & Fitzwater, 1988). In addition to iron, dust and combustion aerosols may also contain Pb and other heavy metals. Ewing et al. (2010) demonstrated a method of quantifying stable Pb isotope ratios in aerosol samples to provide estimates of the proportion of Asian to North American particulate matter. This fingerprinting technique relies on the fact that three naturally occurring isotopes of lead (^{206}Pb, ^{207}Pb, and ^{208}Pb) are formed at differing rates from the radioactive decay of Th and U, the ratio of which is discernably different in Asian and North American crustal materials be it mineral dust, coal, or metal ores (Ewing et al., 2010; Settle & Patterson, 1982). The data from Ewing et al. (2010) suggest an average of 61% ± 12% Asian Pb fraction at Mt. Tamalpais (elevation of 770 m, just upwind of the San Francisco Bay area) from March through May, and in sites throughout Central California and into the Sierra Mountains they found an average of 31% ± 27%. Most of these studies suggest that the bulk of the Asian aerosol mass (diameter ≤ 10 μm) is observed during springtime, although VanCuren (2003) and VanCuren et al. (2005) argue that the transport of Asian dust and smoke aerosols occurs steadily from March–October.

Gaseous pollutants such as tropospheric ozone (O_3), nitrogen oxides (NO_x), and sulfur dioxide (SO_2) frequently accompany the transpacific transport of aerosols (Akimoto, 2003; Cooper et al., 2010; Lin et al., 2015, 2017; Uno et al., 2009) and can contribute to the degraded air quality in many industrial areas. O_3 in particular impairs the human respiratory system and devastates natural ecosystems (Ainsworth et al., 2012; World Health Organization, 2013). Since the 1970s the EPA has sought to control O_3 concentrations in the United Statesand in 2015 updated its ozone attainment standard to <70 ppb 8-hr averages (http://epa.gov). In Great Basin National Park, NV, samples enriched in Asian Pb (>80%; 1.1 ng/m^3), which is enriched in naturally occurring ^{208}Pb compared to North American Pb (Christensen et al., 2015), were collected when O_3 concentrations exceeded background levels by ~5 ppbv. At Whistler Peak, BC, Leaitch et al. (2009) found that Asian aerosol plumes were enriched in O_3 by 10–25 ppbv in spring. Furthermore, baseline O_3 concentrations around the world have increased by about 1%/year over the past 60 years (Parrish et al., 2012). Concentrations of O_3 in the free troposphere reaching the Pacific coast in spring and summer have climbed steadily since the 1980s by 0.3–0.4 ppbv/year (Cooper et al., 2010; Lin et al., 2015), and Lin et al. (2017) assert that median springtime MDA8 O_3 levels at 50% of western U.S. rural monitoring sites have risen by 0.2–0.5 ppbv/year in the period from 1988 to 2014. This increase in baseline O_3 has been

attributed primarily to a rise in Asian NO_x emissions and transpacific transport from East Asia (Lin et al., 2017), yet observational studies quantifying the contribution of exogenous O_3 from Asian air masses to background concentrations (e.g., Christensen et al., 2015; Leaitch et al., 2009) during the summer ozone season are lacking.

Despite the measureable transport of Asian dust and other aerosols to North America, air masses reaching the west coast are often scavenged of aerosols due to cloud processing during uplift and in transit (Brock et al., 2004). These relatively clean, particle free air masses facilitate gas-to particle formation of sulfate (H_2SO_4) in the remote free troposphere (Brock et al., 2004; Dunlea et al., 2009). Along the Pacific coast, the mixing of free tropospheric air with low aerosol surface area with regional soil and biogenic volatile organic compound emissions (BVOCs; Sindelarova et al., 2014) could fuel secondary organic aerosol (SOA) formation within hours (e.g., Claeys, 2004; Kavouras et al., 1998; Went, 1960). Widespread midday particle nucleation such as we show herein may occur all along the west coast of North America, as has been observed across the west coast of Europe in remote regions (Beddows et al., 2014).

This paper characterizes five distinct aerosol types based on composition and transport timescales: Asian dust, Asian combustion aerosols, marine aerosols, local combustion aerosols, and local dust. We quantify the contribution of Asian dust and Asian combustion aerosols to North America and the mean transpacific transport of tropospheric O_3 to the Pacific coast. In addition, we present evidence of local particle nucleation from May to August during periods of onshore airflow near the Pacific coast. We propose that new particle production observed in this study is most likely due to SOA formation from continental BVOC emissions in air masses that have been previously scavenged of other aerosols.

2 Methods

We collected measurements at the Oliver Observing Station operated by the Monterey Institute for Research in Astronomy (MIRA: http://www.mira.org/) on top of Chews Ridge, which is located in the coastal Santa Lucia Mountain Range in Monterey County, California (36.306°N 121.565°W). At 1,550 m, Chews Ridge sits ~1 km above the shallow marine boundary layer that butts up against the coastal mountains about 20 km to the west. Whereas the coastal marine boundary layer is characterized by persistent northwesterly winds during most of the spring throughfall (Dorman et al., 1999), the meteorological setting at Chews Ridge is composed of two dominant wind modes: southwesterly onshore winds (two thirds of the time) and northeasterly offshore winds. The two wind domains are related to the interplay of synoptic forcing from the climatological trough along the California coast that drives southwesterly flow and the thermal low of the Southwestern continental United States, respectively. The latter wind pattern brings polluted air from Central California to the site and typically occurs

during the warmest periods when the thermal low is the strongest and able to overwhelm the prevailing trough pattern at the elevation of the site. The site frequently samples the free troposphere, uninfluenced by North American emissions, particularly when the atmospheric boundary layer overlying the coastal mountains shrinks to a minimum (i.e., during winter or summer nights) and when the site experiences onshore winds.

We collected size-segregated aerosols for elemental analysis with a rotating drum impactor (RDI) nearly continuously from 25 February to 14 September 2012, along with scanning mobility particle size spectra (SMPS, made up of a TSI 3080 electrostatic classifier in line with a TSI 3025A ultrafine condensation particle counter), and O_3 concentrations. Additionally, 24 subsamples of the RDI impactor film were analyzed for Pb isotopic composition. The RDI instrument was mounted on the outside of the second story of the observation station (Figure S1). Ozone and particles were drawn through ¼″ outer-diameter 30′ Teflon (O_3) and a stainless steel (SMPS) inlet lines located ~2 m below the RDI inlet on the west side of the Oliver Observing Station building, ~8 m above the ground. The SMPS, O_3, and data logging computer were housed in a sheltered shed on the first floor.

The RDI instrument is described in detail by Rabbe et al. (1988). Briefly, the instrument advances Mylar sampling strips at a rate of 0.5 mm every 3 hr, yielding an approximate ~3-hr temporal sampling resolution. Particles in theoretical 50% cutoff collection bins based on aerodynamic diameters (5–10 μm, 2.5–5 μm, 1.1–2.5 μm, 0.75–1.1 μm, 0.56–0.75 μm, 0.34–0.56 μm, 0.24–0.34 μm, and 0.09–0.24 μm) were autonomously collected on Mylar strips of eight stages for ~5–6 weeks prior to retrieval and replacement. RDI samples corresponding to each of eight size classes of aerosols were analyzed for elemental composition using X-ray fluorescence (XRF) technology at the Advanced Light Source-Lawrence Berkeley National Laboratory. Mylar strips were coated with Apiezone grease to reduce particle bounce during collection. The aerosol concentration (ng/m^3) of each sample was calculated using the RDI instrument's flow rate (15 L/min) and advance rate. XRF measurements were conducted twice to test the precision of the elemental composition analysis. At select (nonrandom) dates, 8 mm sections (i.e., approximately two days) of Mylar films were subsampled for Pb isotopic analysis following XRF analysis and analyzed for light absorption (VanCuren & Gustin, 2015). Although issues of accuracy and exact sizing determination have been raised with respect to the RDI (Venecek et al., 2016; Wexler et al., 2015), especially under low particulate matter loadings, the XRF temporal patterns of elements from the RDI sampling have been shown to generally agree with other methods (Wexler et al., 2015). We propose that the results of our RDI-XRF analyses does not depend on exact concentrations or size distributions but rather on relative distributions of these elements, and thus are not contingent on highly precise quantification of size speciated aerosols.

We conducted a positive matrix factorization (PMF) analysis of the RDI-XRF data using the Environmental Protection Agency 5.0 software, which is a

weighted least squares solution to the multivariate receptor problem yielding factor (source) profiles and temporal contributions of these sources to each time series observation. Although the resulting factors are not orthogonal, this model has low rotational ambiguity and produces factors that are more easily interpreted due to inherent nonnegativity constraints on the solution (Kim & Hopke, 2005). We selected the elements Al, Ca, Cl, Fe, K, Mo, Na, Pb, S, Si, and Ti based on their crustal, combustion, or marine abundance and a low average signal-to-noise ratio (S/N > 5), which are deemed strong predictor variables (Paatero et al., 2002). Model runs were initiated with random seeds and relied on two inputs, the mean concentrations of duplicate samples at each time-point and the corresponding analytical uncertainty of each XRF measurement. In two of four sampling periods, critical orifices of the cartridges were improperly installed between the fifth and sixth stages (Venecek et al., 2016), yielding sampling errors in these stages. Therefore, stages 5 and 6, corresponding to aerosol sizes ~0.56–0.75 µm and 0.34–0.56 µm, were not used in this analysis. A total of 100 runs converged, each yielding six positive matrix factors. The model run with the best goodness-of-fit statistics was selected, residuals of each element were inspected for skew and heavy-tails, and the selected run was further analyzed using native EPA software Bootstrap and Fpeak methods to verify that the initial factor profiles and contributions were robust and that the PMF solution had low rotational ambiguity (Bootstrap and Fpeak solutions differed little from the base results). We examined the timing of transport events using each factor contributions' power spectra, calculated after the application of a Hamming window to minimize distortion due to sidelobe spectral leakage. We also calculated the top 10% of each factor's contributions and characterize the particle distribution of each factor.

The Pb isotopic composition ($^{206}Pb/^{207}Pb$ and $^{208}Pb/^{207}Pb$) of aerosol samples was measured by multicollector-inductively coupled plasma-mass spectrometer (ICP-MS) to further identify aerosol origins (e.g., Christensen et al., 2015; Ewing et al., 2010). Pb isotope subsamples from Mylar strips, representing approximately two days or 16 ~3 hr samples, were leached in 6 N HCl in Teflon vials on a hot plate set to 90 °C for 4 hr. After cooling the Mylar strips were removed, and the leachates dried down and taken up again in 0.5 N HBr for chemical separation on small-volume columns using AG1x8 resin eluted with 0.5 N HBr. Pb was stripped off with 6 N HCl. Pb from subsamples was then dried down and taken up in 0.3 N HNO_3 and spiked with the appropriate amount of Tl solution as determined by a concentration measurement on a 10% sample aliquot. The Pb isotopic compositions were measured on a Neptune + ICP-MS using the $^{203}Tl/^{205}Tl$ ratio for mass fractionation correction. This method has been applied extensively to distinguish Asian Pb from Pb derived from North American sources (e.g., Figure 1; Bollhöfer & Rosman, 2001, 2002; Christensen et al., 2015; Díaz-Somoano et al., 2009; Ewing et al., 2010; Tan et al., 2006). The percent of Asian influence is calculated as the ratio of ▲ ^{208}Pb observed/▲ ^{208}Pb Asia,

where ▲ ^{208}Pb denotes the difference between the expected California ^{208}Pb/^{207}Pb ratio and either the observed or the expected Asian ^{208}Pb/^{207}Pb ratio for a given ^{206}Pb/^{207}Pb ratio (Figure 1; Ewing et al., 2010).

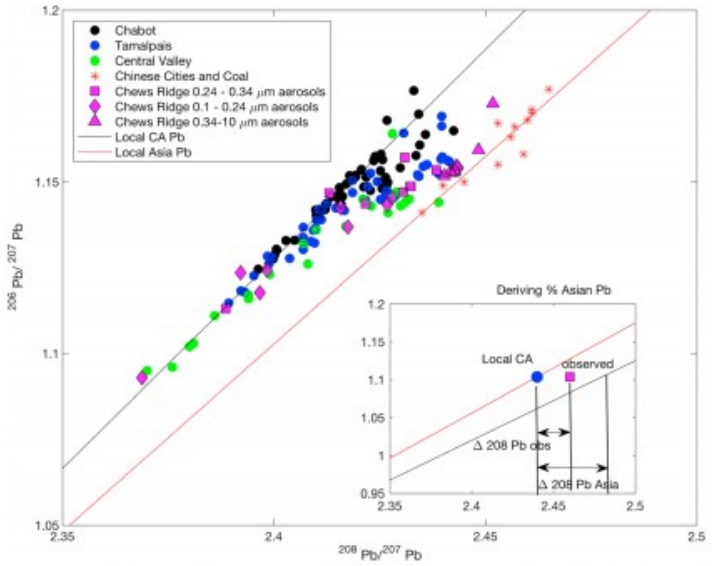

Figure 1. Compilation of Pb isotope data from XRF-RDI samples from Chews Ridge, as well as samples from throughout northern and central California and Asia. Inset illustrates how the %Asian Pb (of total Pb) is derived. Data from Bollhöfer and Rosman (2001, 2002), Tan et al. (2006), Díaz-Somoano et al., 2009, and Ewing et al. (2010).

Particle size spectra measurements were made using a SMPS between 12 May and 31 August 2012 at an ~5-min temporal resolution. Particles were counted in 107 diameter size class bins ranging between 14 and 650 µm. Raw data were corrected for particle losses through the inlet calculated at each diameter according to the Particle Loss Calculator software tool (von der Weiden et al., 2009), which for the system described above lead to an estimated 50% cutoff at 16 nm aerodynamic diameter, and 90% efficiency at 72 nm. Thereafter, data were binned to a temporal resolution of 1 hr for comparison with ozone and meteorological data. Data were segregated based on hourly-average vector wind direction and wind speed into onshore (150–330° degrees; >1 m/s) and offshore (330–150°; >1 m/s) measurements. Due to a combination of SMPS and weather station instrument troubles data are missing from two ~10-day periods between 12–22 July and 16–27 August, as well as data between 19 May and 23 June. We formalized the identification of nucleation events following the approach of Heintzenberg et al. (2007), quantifying nucleation mode particle number and Aitken/aged nucleation mode median diameter. Thresholds adopted for the nucleation mode (<50 nm) and the Aitken/aged nucleation mode (<200 nm) were based on the particle concentration plots and generally resemble those reported by Beddows et al. (2014) for mountain and western sites in Europe. Each nucleation event was treated separately, and nucleation particle number and Aitken/aged nucleation mode median particle diameter from 11 a.m. to 5 p.m. were correlated with the total surface area (preceding

nucleation events; from 5 a.m. to 11 a.m.) to test if particle formation occurred in clean, prescavenged air masses.

In addition to measurements of airborne particles, we obtained measurements of O_3, and local meteorological data. O_3 concentrations were measured using the 2B technologies Ozone Monitor (Model 202, which was calibrated every three to four months). Air sampled for O_3 measurements was filtered through a 47 mm Teflon Particle Filter, replaced every three to six months as required. Final O_3 data products represent compiled 1-hr averages of raw O_3 data that were vetted by eye for any periods of degraded performance based on the flow, lamp intensity, pressure, and temperature diagnostic variables. The seasonal cycle was removed from the O_3 data using an ongoing time series at Chews Ridge prior to its use statistical correlations. Ancillary meteorological data were provided courtesy of the Oliver Observing Station at Chews Ridge, supported by MIRA. Wind speed, wind direction, temperature, and relative humidity measurements collected at Chews Ridge by a Davis weather station are available at a 5-min temporal resolution.

3 Results and Discussion

3.1 PMF Results and Source Apportionment

On average, the PMF model reproduced observed species well ($r = 0.71 \pm 0.03$), given that a few factors are not capable of reproducing all the observed variance. In addition, the Kolmogorov-Smirnoff test indicated the residuals were normally distributed for 98.5% of species, and >95% of species from the base run were within the inner quartile range of Bootstrap intervals and Fpeak results, suggesting that this solution was not particularly sensitive to random errors or rotational ambiguity. Factor contributions and profiles, both of which were normalized to one, facilitated factor profile interpretability and source apportionment. The PMF analysis yielded five identifiable factors (of six) based on factor profiles: Asian dust, (aged) Asian combustion, marine, local dust, and local combustion (Table 1 and Figures 2 and S3). One of the six factors, factor 4, was not interpretable (i.e., was considered an artifact of the data collection) and is not shown. Factors differed in their particle distributions as well as in their elemental composition (Figure S2 and Table 1). Seasonally, we found that March-April-May (MAM) and June-July-August-(September) (JJA(S)) contain 89% and 10%, respectively, of the contributions from the Asian dust factor, whereas MAM and JJA(S) contained 51% and 44% (45%), respectively, of contributions from the Asian combustion factor (Table 1).

Table 1

The Name, PMF Number, the Particle Distribution Mode, the Mean Squared Error (MSE) of the Elemental Bulk Ratios Belonging to Each Factor Profile Compared to Elemental Ratios of Dust Attributed to Transpacific Transport (Holmes & Zoller, 1996), the Relationship to Pb From Asia and Deseasonalized O_3, and the Contribution (%) That Occurred in Spring (MAM, With the Remaining Contribution Occurring in JJAS)

Name	Number	Aer. Mode	MSE H&Z	%Asian Pb. Rel.	Deseason. O_3 Rel.	MAM
Asian dust	2	59.4 nm	0.08	$r = 0.80, p < 0.001$ Pb = 19.1 + 2.7 AD	$r = 0.24, p < 0.001$ O3 = −3.2 + 1.5xAD	89%
Asian combustion	6	55.2 nm	0.13	$r = 0.75, p < 0.001$ Pb = −4.0 + 23.1xAC	$r = 0.24, p < 0.001$ O3 = −3.8 + 2.8xAC	51%
Marine	5	63.8 nm	9.9E + 4	$r = -0.26, p = 0.22$ Pb = 54.7–7.8xM	$r = 0.16, p < 0.01$ O3 = −3.1 + 1.7 M	59%
Local dust	3	59.4 nm	93	$r = -0.30, p = 0.16$ Pb = 74.3–28.4xLD	$r = 0.02, p = 0.45$	37%
Local combustion	1	41.3; 55.2 bimodal	0.65	$r = -0.84$, p < 0.001 Pb = 74.6–30.7xLC	$r = -0.07, p = 0.04$	22%

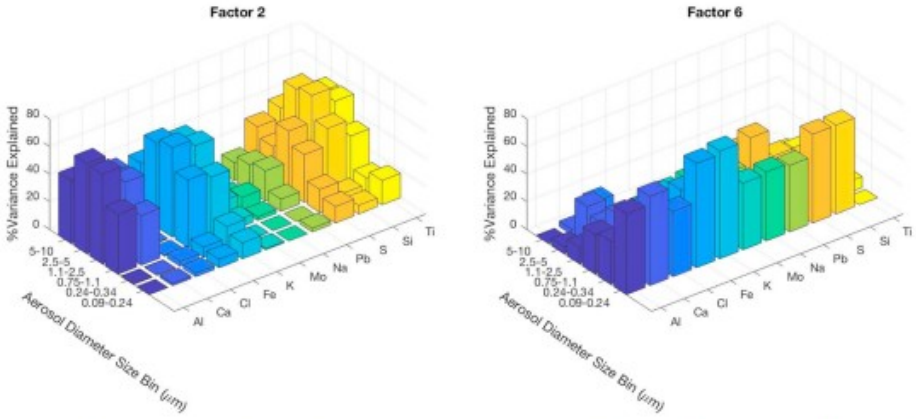

Figure 2. Profiles of factors 2 and 6, determined using EPA 5.0 positive matrix factorization. Factor 2 attributed to Asian dust and factor 6 attributed to Asian combustion and stovetop burning.

Factor 2, the Asian dust factor, summarized ~40–60% of the crustal elements (e.g., Ca, Fe, Si, and Ti) in coarse (D_p > 2.5 μm) aerosols, typically associated with dust (Figure 2a; VanCuren et al., 2005). Factor 6, the Asian combustion factor, explained a substantial percent of elements S, K, and Pb in fine aerosols (≤1 μm; Figure 2b). S and K are produced from combustion and metallurgy (Nriagu, 1990; VanCuren, 2003; VanCuren et al., 2005). The marine factor, factor 5, accounted for a high percentage of Cl, S, and Na (Figure S3), which are known to be principal components of sea salt aerosols. Factors 1 and 3, which were dubbed the local combustion factor and the local dust factor explained 40–60% of the crustal elements (e.g., Al, Ca, Fe, Si, and Ti) in the largest size class bin (5–10 μm), approximately seven times more than the Asian dust factor (Figure S3). Following Holmes and Zoller (1996), we also examined the ratio of crustal elements Ca, Fe, K, Na, and Ti (summed across all available size bins and normalized to total Al) in each factor. The ratios of the Asian dust factor in this study agreed well with literature values (Figure S4 and Table 1); however, this agreement, interpreted based on mean squared error, worsened in order of the following factors: Asian combustion, local combustion, local dust, and marine (Table 1). In addition to distinct compositions, differences in the particle distribution modes of factors denote subtle size differences between dust, combustion,

and marine fine aerosols (Figure S2 and Table 1). In particular, the local combustion factor has a bimodal particle distribution, potentially indicative of local particle nucleation.

3.2 PMF Versus Pb Isotope Subsamples

Seeking to minimize the number of expensive and time-intensive $^{208}Pb/^{207}Pb$ versus $^{206}Pb/^{207}Pb$ measurements, we carefully chose subsamples from archived Mylar films based on (and to corroborate) our PMF results (Figure 3). Overall, we found good agreement between the percent of Asian Pb calculated from Pb isotope measurements and the temporal contributions of the Asian combustion factor and Asian dust factor derived from the PMF analysis (Figure 3). These independent measurements both suggest that Asian influence exhibits a strong springtime pulse, which in 2012 peaked on 12 April. Indeed, numerous studies have noted a spring pulse in the contribution of Asian dust (and to a lesser extent combustion aerosols) to North America (Uno et al., 2009; Yu et al., 2012), and some modeling and field-based studies indicate that Asian transport continues into the summertime (e.g., Holzer & Hall, 2007; VanCuren, 2003; VanCuren et al., 2005).

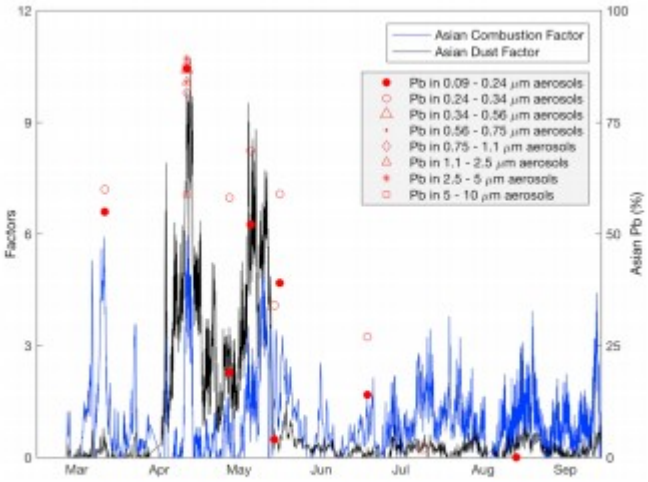

Figure 3. Time-series of the % Asian Pb derived from Pb isotope analysis and the PMF signals.

Six of the 20 subsections from the RDI record targeted a period of peak Asian influence in April and were probed for differences in $^{208}Pb/^{207}Pb$ versus $^{206}Pb/^{207}Pb$ of different sized aerosols (Figure 3). A wide range of aerosol sizes (0.09–5 μm) contained very high concentrations of Pb in the 12 April sample (86 ± 2.6% Asian Pb) with the exception of aerosols in the largest size class bin (5–10 μm), which contained 59% Asian Pb (Figure 3). The 5–10 μm aerosols may have been strongly influenced by gravitational settling or wet/dry deposition in the marine boundary layer during transit. Wet deposition due to below-cloud scavenging and in-cloud scavenging is thought to be orders of magnitude higher in the marine boundary layer than in the

free troposphere, particularly for aerosols ≥5 μm (e.g., Croft et al., 2014; Zhao, 2003). As suggested by Brock et al. (2004) gravitational settling could also play a small role in the removal of larger aerosols, leading to ~1 km vertical displacement during transit at 600 mb 263 K. Similarly, throughout the spring and summer, the percent of Asian influence in each of the smallest two size classes was well correlated with one another (r = 0.89, p < 0.01), and we observed little difference between the two (15.5 ± 14% higher Asian influence in the smallest size bin; data not shown).

We found a strong correlation between the percent of Asian Pb across all size classes and the Asian dust factor (Figure 4a) and the Asian combustion factor (Figure 4b). Because each PMF is normalized to an average value of unity, the slope is used to estimate the average contribution of the Asian combustion factor to Asian Pb. Together, these factors suggest that transcontinental transport is responsible for approximately 31% Asian Pb at Chews Rigde on average (8.3% was attributed to the Asian dust factor, and 23.1% was attributed to the Asian combustion factor), while 15% (19.1% - 4.1%) Asian Pb is not explained by our PMF results. We speculate that this unexplained Asian Pb fraction may be linked to the fine-aerosol global background connected with Asian emissions (e.g., Vernier et al., 2015). Thus, an average of 46% of the Pb observed at Chews Ridge during this experiment was of Asian origin, which is in line with the average observed by Ewing et al. (2010) at Mt. Tamalpais (44%) along the coast north of San Francisco, and at various sites within the Central Valley (31%). As might be expected, Asian Pb was negatively correlated with the local combustion factor and the local dust factor (Table 1).

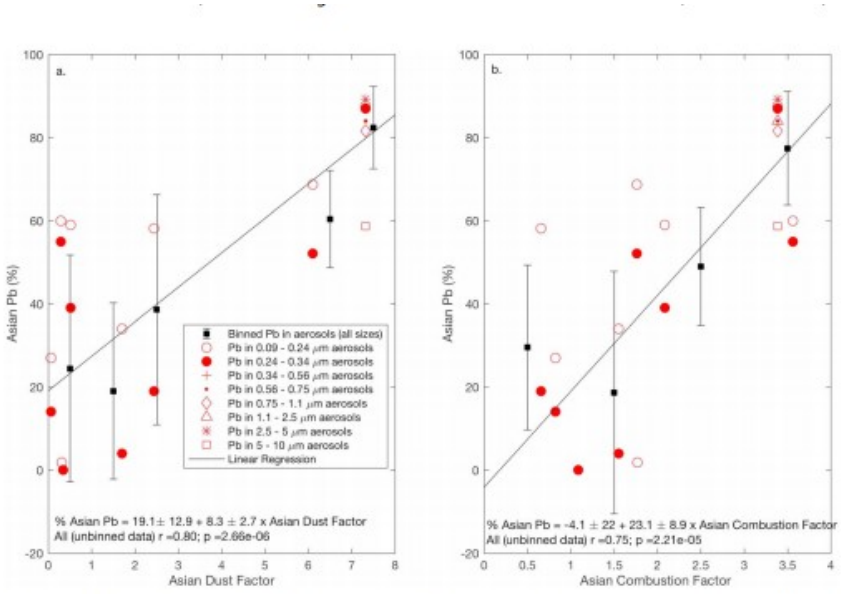

Figure 4. The relationship between Asian Pb (%) and (a) the Asian dust factor and (b) the Asian combustion factor across all aerosol bin sizes. For reference, raw data are binned per unit of factor contributions.

3.3 The Transcontinental Transport of Ozone

The Asian PMFs provide a continuous estimate of the Asian influence in 2012 to determine the associated O_3 originating from Asian emissions. We observed a positive correlation between deseasonalized O_3 and the Asian dust (Figure 5a) and combustion factors (Figure 5b). Similarly, the slope in these relationships was used to calculate the increase in O_3 attributable to the Asian combustion factor, 2.8 ppbv, and the Asian dust factor 1.5 ppbv (Figure 5 and Table 1).

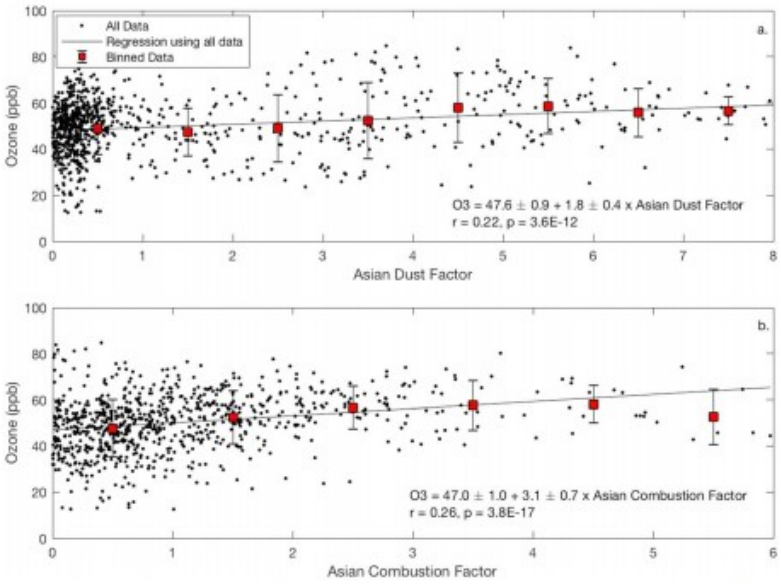

Figure 5. The regression of ozone (ppb) against the (a) Asian dust factor and the (b) Asian combustion factor (n = 1,015). Binned data (mean and SD) are also shown for reference (b).

PMF signals were also used to estimate the transport of O_3 to the Pacific Coast Range, where comprehending the benefits of regional policies relies on a quantitative understanding of large-scale atmospheric dynamics. The above Asian transport events contribute a total 4.3 ± 0.80 ppb (Asian combustion plus Asian dust factor), which combined with an additional 2.0 ppb from the unexplained Asian Pb fraction (note that the Asian combustion and Asian dust factors only accounted for 68% of the Asian Pb observed, and thus, we assume 68% of the O_3 due to transcontinental transport, as well), which is equal to 6.3 ± 0.80 ppb ppb O_3 above background. This result is in general agreement with the 5 ± 5.5 ppbv contribution of Asian O_3 found by Christensen et al. (2015) during discrete episodes at 2 km elevation in Eastern Nevada. Further, our observationally derived enhancement is similar to the ~5–6 ppb mean Asian O_3 predicted for May–June of 2010 by the Geophysical Fluid Dynamics Laboratory chemistry-climate model, AM3 (~50 km resolution), at 800 hPa (Lin et al., 2012, Figure 9a). However, it is significantly greater than the surface level enhancements of ~3.5 ppb predicted by Lin et al. (2012, their Figure 9b), which points to the importance of the mesoscale boundary layer dynamics in complex terrain when it comes to entrainment of transpacific plumes down to the surface. Due to the labor and cost required to analyze Pb isotope samples, however, previous studies

quantifying the contribution of Asian influence to Pb or O_3 (e.g., Christensen et al., 2015; Ewing et al., 2010) have relied on relatively few observations (<100). This study supports these earlier findings using a correlation between O_3 and factor contributions of Asian dust and combustion influences from RDI-XRF data, yielding >1,000 concurrent observations between February and September 2012.

3.4 Transport Times and Geographic Origin

We used power spectra and the National Oceanic and Atmospheric Administration Hybrid Single-Particle Lagrangian Integrated Trajectory (HYSPLIT) particle dispersion model, in addition to total column CO retrievals from the Atmospheric IR Sounder (AIRS) satellite instrument to probe the transport timescales and geographic origin of air masses observed at Chews Ridge. PMF contributions can be used to elucidate the transport timescales of the Asian dust factor and the Asian combustion Factor (Figure 6), as well as other factors (Figure S5). Power spectra of the PMF factors illustrate distinct transport mechanisms for Asian combustion, Asian dust, marine, and local signals (Figures 6; Figure S5). The transport of the Asian dust factor is dominated by seasonal (springtime) and monthly periodicities. In other words, while the Asian dust does come at regular monthly episodes throughout the year, it is heavily peaked in the springtime as pointed out by several previous researchers (Liang, 2005; VanCuren, 2002). Liang (2005) use the GEOS-CHEM model to report that on average a “long range transport” event occurs every 30 days in the lower troposphere above Northwestern Washington state, corresponding well with our finding of the Asian dust factor's periodicity. On the other hand, transport of the Asian combustion factor occurs more characteristically of scalars in the free troposphere having an approximate −5/3 power slope (Nastrom & Gage, 1985) on timescales of 4–20 days (Figure 6). These results are broadly concordant with previous studies, which suggest episodic transport through the troposphere every 10–30 days throughout the spring and summer (e.g., Holzer et al., 2005; Jaffe et al., 2003; Liang, 2005; Liang et al., 2007), and a large springtime pulse of Asian Dust when transport is accelerated due to high zonal winds (Ewing et al., 2010; Holmes & Zoller, 1996; Uno et al., 2009; Yu et al., 2012). Results from the HYSPLIT back trajectories suggest that particles observed on 12 April 2012 during a short-lived period of strong Asian influence traveled over Northeastern China ~8 days prior to reaching Chews Ridge (Figure 7). Averaged ascending and descending (day and night) CO retrievals from AIRS on 11 April, one day prior to the large event observed on 12 April, show a substantial CO enhancement adjacent to Chews Ridge (Figure S6b). The other retrieval shown in Figure S6a is from a period with minimal Asian influence according to the PMF analysis (Figure 3), which correspondingly shows no significant CO plumes in the Eastern Pacific. CO has been used previously as a tracer of Asian pollution to forecast high ozone (Lin et al., 2012), and here corroborates that the air mass observed on 12 April 2012 was very likely of direct Asian origin. In comparison, the

transport frequency of local and marine aerosols to the west coast of North America has been less well characterized, but higher frequency transport is expected due to shorter transport distances, and presumably shorter transit times. Indeed, we found that the local dust factor, the local combustion factor, and the marine factor exhibited frequent transport on timescales of 1–6 days (Figure S5).

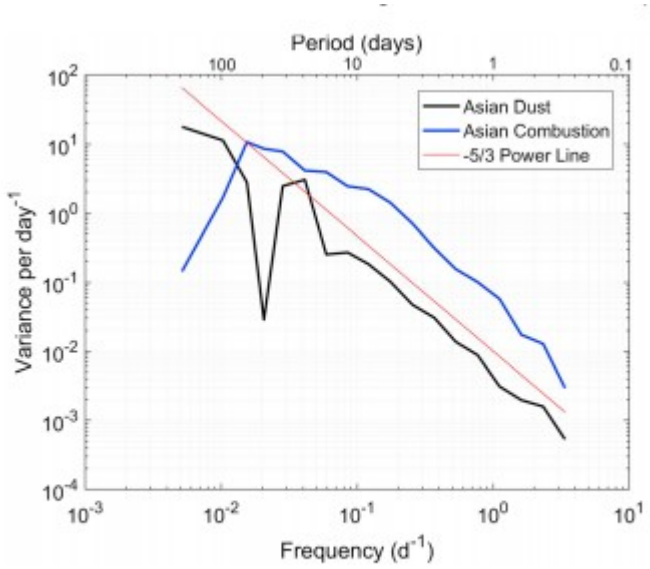

Figure 6. Spectral density plots of factor 2-Asian dust and factor 6-Asian combustion. Data are filtered using a hamming filter with a cutoff frequency of 6.5/day.

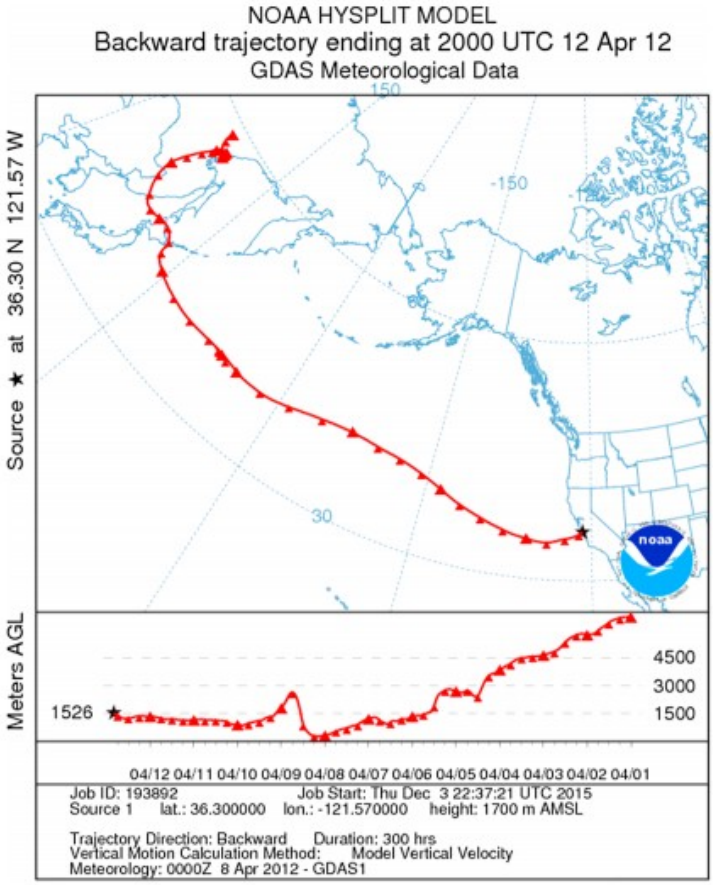

Figure 7. NOAA HYSPLIT back trajectory at the peak of the Asian influence (04/12). Peak Asian influence is determined using both Pb isotopes and PMF factors (see Figure 3).

3.5 Particle Nucleation

In addition to the transport of foreign aerosols, spring and summertime particle nucleation represents an important source of secondary aerosols to Chews Ridge and regions downwind. We present evidence of onshore particle nucleation in the diurnal pattern of the particle size and number (Figures 8a and 8b), the so-called banana curves, for onshore wind conditions. The onset of particle nucleation occurs around noon, intensifies until ~2:00 p.m., and is followed by the subsequent growth of existing particles and an increase in the overall surface area between 2 p.m. and 5 p.m.. We observe a nearly bimodal distribution in the daytime onshore particle number distribution as a function of aerosol size (Figure 8b), with a mode near 35 nm as well as the more typical mode around 60 nm. At nighttime, one mode of Aitken/aged nucleation particles was present, which had overall lower particle number and surface area than its daytime counterpart (Figures 8b and 8c). Corresponding offshore diurnal particle number concentration and particle number plots demonstrate that particle nucleation was not observed during periods of offshore flow (Figures 8d and 8e). Only one mode of Aitken/aged particles was present under these conditions day or night and shared similar particle number characteristics.

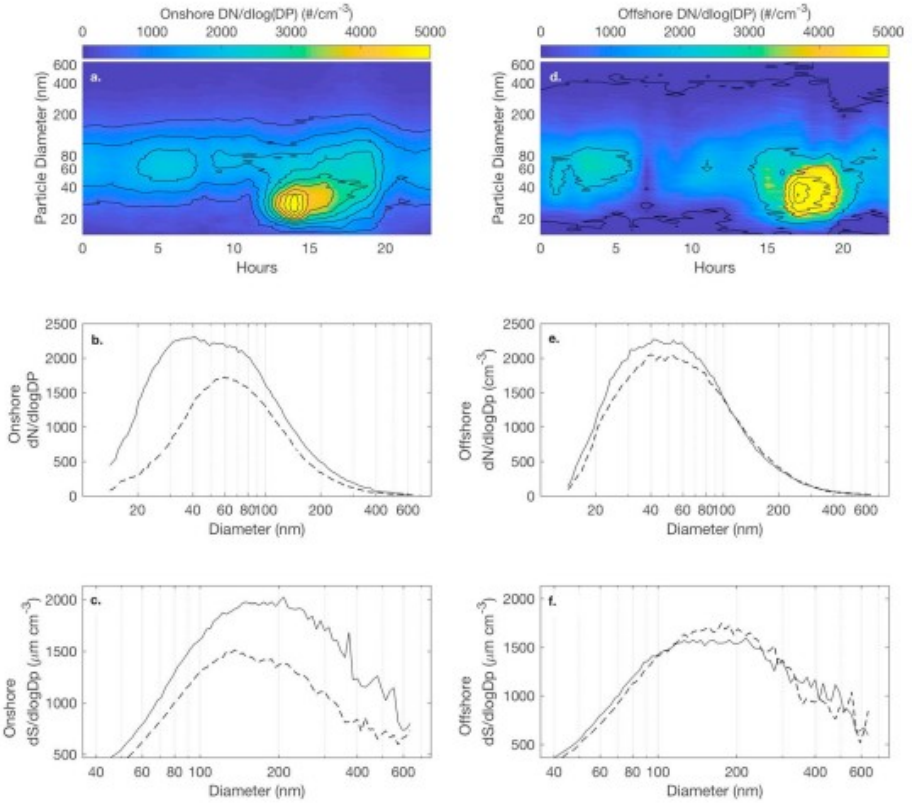

Figure 8. (a) Diurnal particle number concentration plots during periods of onshore and (d) offshore flow. Contours mark statistically significant differences (i.e., mean differences greater than the standard error); (b) daytime (solid lines) and nighttime (dashed lines) particle number and (c) particle surface area as a function of aerosol size diameter during periods of onshore flow and similarly (e and f) for periods of offshore flow.

To test the hypothesis that onshore particle nucleation occurs in air masses that have been previously scavenged of particles through transpacific transit, we correlated the overall surface area from the preceding morning (5 a.m.–11 a.m.) with particle nucleation number (and Aitken/aged aerosol mode median size) on the same day (11 a.m.–5 p.m.). Inherent is the assumption that our SMPS measurements capture the majority of the surface area present. Although other, larger aerosol modes may contribute to the total surface area, our SMPS measurement depict the bulk of the surface area from the nucleated and Aitken/Aged aerosol modes during both periods of onshore and offshore flow (Figures 8c and 8f). We observed a statistically significant inverse relationship between the overall surface area in the morning and the nucleation particle number measured during the following afternoon (Figure 9a). Correspondingly, the median size of nucleation and Aitken/aged particles was positively correlated with overall surface area that morning (and negatively correlated with nucleation particle number; Figure 9b). We did not observe statistically significant relationships between O_3 concentrations and temperature with either nucleation particle number or the median size of nucleation and Aitken/aged particles.

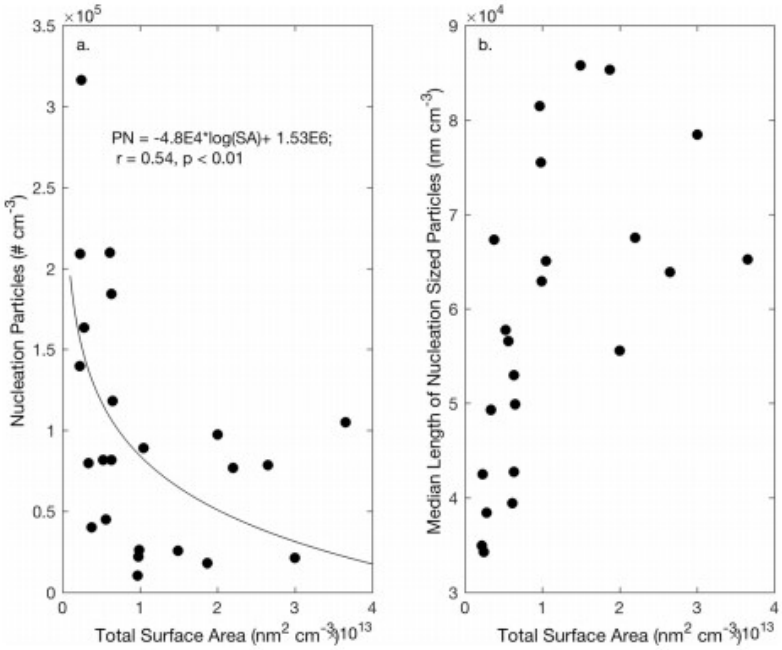

Figure 9. Relationship between (a) the total surface area of particles from 5 a.m. to 11 a.m. and particle number of nucleation-mode particles between 11 a.m. and 5 p.m., and (b) the median diameter length of nucleation and accumulation mode particles between 11 a.m. and 5 p.m. in 2012.

Our data suggest that particle nucleation occurs on summer afternoons in air masses that have been prescavenged of existing aerosols (Figures 8 and 9). Because this process is exclusively observed during the daytime, we conclude that this secondary aerosol formation is driven by the OH oxidation. Isoprene and α-pinene and β-pinene (two monoterpene isomers) emissions, which are correlated with light and sensible heat flux (Jardine et al., 2015; Rinne et al., 2002), could fuel SOA production through OH oxidation on the order of a few hours (e.g., Atkinson, 1997). Indeed, Sindelarova et al. (2014) suggest that α- and β-pinene and isoprene represent the most important local sources of BVOCs near Chews Ridge (~1–3 ppbv). We propose that the west coast of North America satisfies the requirement for widespread, rapid nucleation events: (1) relatively clean (particle-free) air during periods of onshore flow, (2) plentiful sunshine due to the Pacific High fueling the photolysis production of OH, (3) local boreal BVOC and soil NOx emissions (~1 ppb), and (4) warm temperatures, leading to elevated reaction rates.

4 Conclusions

Our observations point to the transport of distinct Asian dust and Asian combustion plumes. Seasonally, MAM accounts for the lion's share (89%) of the contributions in the Asian dust signal, but half (~51%) of the contributions in the Asian combustion signal, compared with JJA(S). We conclude that Asian dust and combustion aerosols are responsible for at least 46% of the Asian Pb and 6.5 ppb O_3 observed at Chews Ridge during our study period. Nearby particle nucleation provides an additional source of fine secondary aerosols to Chews Ridge on spring and summer (May–September) afternoons. We hypothesize that this secondary aerosol

formation is driven by a combination of photochemistry, continental BVOC emissions, and onshore air masses with low preexisting aerosol surface area. Our results indicate that PMF analysis of XRF RDI data can provide a useful and inexpensive complementary tool to more time-intensive methods, such as Pb isotope analysis, to investigate the transport of foreign aerosols and gas-phase pollutants. This study suggests that Chews Ridge would prove an excellent location for long-term observations of background O_3 and aerosols transport to the Pacific Coast.

Acknowledgments

In particular, we would like to thank MIRA for the use of meteorological data and logistical support in deploying the RDI sampler, O_3 monitor, and SMPS at the Oliver Observing Station on Chews Ridge. We would also like to thank UC Davis PhD student Yiting Li for her correction of raw SMPS data for particle loss. Data for this study are uploaded as supporting information, and questions may be directed by e-mail with the corresponding author. Support for the Center for Isotope Geochemistry at LBNL is provided by the Department of Energy, Office of Basic Energy Sciences through contract DE-AC02-05CH11231 to Lawrence Berkeley National Laboratory. This work was made possible by grants from the San Joaquin Valley Air Pollution Control District and University Affiliated Research Center's Aligned Research Program grant NAS2-03144. This research used resources of the Advanced Light Source, which is a DOE Office of Science User Facility under contract no. DE-AC02-05CH11231. I. F.’s effort is supported by the California Agricultural Experiment Station, Hatch project CA-D-LAW-2229-H.

References

Ainsworth, E. A., Yendrek, C. R., Sitch, S., Collins, W. J., & Emberson, L. D. (2012). The effects of tropospheric ozone on net primary productivity and implications for climate change. *Annual Review of Plant Biology*, 63(1), 637–661. https://doi.org/10.1146/annurev-arplant-042110-103829

Akimoto, H. (2003). Global air quality and pollution. *Science*, 302(5651), 1716– 1719. https://doi.org/10.1126/science.1092666

Atkinson, R. (1997). Gas-phase tropospheric chemistry of volatile organic compounds: 1. Alkanes and alkenes. *Journal of Physical and Chemical Reference Data*, 26(2), 215. https://doi.org/10.1063/1.556012

Beddows, D. C. S., Dall'Osto, M., Harrison, R. M., Kulmala, M., Asmi, A., Wiedensohler, A., et al. (2014). Variations in tropospheric submicron particle size distributions across the European continent 2008–2009. *Atmospheric Chemistry and Physics*, 14(8), 4327– 4348. https://doi.org/10.5194/acp-14-4327-2014

Bollhöfer, A., & Rosman, K. J. (2001). Isotopic source signatures for atmospheric lead: The northern hemisphere. *Geochimica et Cosmochimica Acta*, 65(11), 1727– 1740. https://doi.org/10.1016/S0016-7037(00)00630-X

Bollhöfer, A., & Rosman, K. J. (2002). The temporal stability in lead isotopic signatures at selected sites in the southern and northern hemispheres. *Geochimica et Cosmochimica Acta*, 66(8), 1375– 1386. https://doi.org/10.1016/S0016-7037(01)00862-6

Brock, C. A., Hudson, P. K., Lovejoy, E. R., Sullivan, A., Nowak, J. B., Huey, L. G., et al. (2004). Particle characteristics following cloud-modified transport from Asia to North America: Cloud-modified transport from Asia. *Journal of Geophysical Research*, 109, D23S26. https://doi.org/10.1029/2003JD004198

Christensen, J. N., Weiss-Penzias, P., Fine, R., McDade, C. E., Trzepla, K., Brown, S. T., & Gustin, M. S. (2015). Unraveling the sources of ground level ozone in the Intermountain Western United States using Pb isotopes. *Science of the Total Environment*, 530-531, 519– 525. https://doi.org/10.1016/j.scitotenv.2015.04.054

Claeys, M. (2004). Formation of secondary organic aerosols through photooxidation of isoprene. *Science*, 303(5661), 1173– 1176. https://doi.org/10.1126/science.1092805

Cooper, O. R., Parrish, D. D., Stohl, A., Trainer, M., Nédélec, P., Thouret, V., et al. (2010). Increasing springtime ozone mixing ratios in the free troposphere over western North America. *Nature*, 463(7279), 344– 348. https://doi.org/10.1038/nature08708

Croft, B., Pierce, J. R., & Martin, R. V. (2014). Interpreting aerosol lifetimes using the GEOS-Chem model and constraints from radionuclide measurements. *Atmospheric Chemistry and Physics*, 14(8), 4313– 4325. https://doi.org/10.5194/acp-14-4313-2014

Díaz-Somoano, M., Kylander, M. E., López-Antón, M. A., Suárez-Ruiz, I., Martínez-Tarazona, M. R., Ferrat, M., et al. (2009). Stable lead isotope compositions in selected coals from around the world and implications for present day aerosol source tracing. *Environmental Science & Technology*, 43(4), 1078– 1085. https://doi.org/10.1021/es801818r

Dorman, C. E., Holt, T., Rogers, D., & Edwards, K. (1999). Large-scale structure of the June–July 1996 marine boundary layer along California and Oregon. *Monthly Weather Review*, 128, 1632– 1652.

Duce, R. A., Unni, C. K., Ray, B. J., Prospero, J. M., & Merrill, J. T. (1980). Long-range atmospheric transport of soil dust from Asia to the tropical North Pacific: Temporal variability. *Science*, 209(4464), 1522– 1524. https://doi.org/10.1126/science.209.4464.1522

Dunlea, E. J., DeCarlo, P. F., Aiken, A. C., Kimmel, J. R., Peltier, R. E., Weber, R. J., et al. (2009). Evolution of Asian aerosols during transpacific transport in INTEX-B. *Atmospheric Chemistry and Physics*, 9(19), 7257– 7287. https://doi.org/10.5194/acp-9-7257-2009

Ewing, S. A., Christensen, J. N., Brown, S. T., Vancuren, R. A., Cliff, S. S., & Depaolo, D. J. (2010). Pb isotopes as an indicator of the Asian contribution to

particulate air pollution in urban California. *Environmental Science & Technology*, 44(23), 8911– 8916. https://doi.org/10.1021/es101450t

Fischer, E. V., Perry, K. D., & Jaffe, D. A. (2011). Optical and chemical properties of aerosols transported to Mount Bachelor during spring 2010. *Journal of Geophysical Research*, 116, D18202. https://doi.org/10.1029/2011JD015932

Hadley, O. L., Corrigan, C. E., Kirchstetter, T. W., Cliff, S. S., & Ramanathan, V. (2010). Measured black carbon deposition on the Sierra Nevada snow pack and implication for snow pack retreat. *Atmospheric Chemistry and Physics*, 10(15), 7505– 7513. https://doi.org/10.5194/acp-10-7505-2010

Heintzenberg, J., Wehner, B., & Birmili, W. (2007). “How to find bananas in the atmospheric aerosol”: New approach for analyzing atmospheric nucleation and growth events. *Tellus B*, 59(2), 273– 282. https://doi.org/10.1111/j.1600-0889.2007.00249.x

Holmes, J., & Zoller, W. (1996). The elemental signature of transported Asian dust at Mauna Loa observatory. *Tellus B*, 48(1), 83– 92. https://doi.org/10.1034/j.1600-0889.1996.00008.x

Holzer, M., & Hall, T. M. (2007). Low-level transpacific transport. *Journal of Geophysical Research*, 112, D09103. https://doi.org/10.1029/2006JD007828

Holzer, M., Hall, T. M., & Stull, R. B. (2005). Seasonality and weather-driven variability of transpacific transport. *Journal of Geophysical Research*, 110, D23103. https://doi.org/10.1029/2005JD006261

Hu, Z., Zhao, C., Huang, J., Leung, L. R., Qian, Y., Yu, H., et al. (2016). Trans-Pacific transport and evolution of aerosols: Evaluation of quasi-global WRF-Chem simulation with multiple observations. *Geoscientific Model Development*, 9(5), 1725– 1746. https://doi.org/10.5194/gmd-9-1725-2016

Huang, R.-J., Zhang, Y., Bozzetti, C., Ho, K.-F., Cao, J.-J., Han, Y., et al. (2014). High secondary aerosol contribution to particulate pollution during haze events in China. *Nature*, 514(7521), 218– 222. https://doi.org/10.1038/nature13774

Intergovernmental Panel on Climate Change (2014). *Climate change 2013—The physical science basis: Working Group I Contribution to the Fifth Assessment Report of the Intergovernmental Panel on Climate Change*. Cambridge: Cambridge University Press. Retrieved from http://ebooks.cambridge.org/ref/id/CBO9781107415324

Jaffe, D., McKendry, I., Anderson, T., & Price, H. (2003). Six “new” episodes of trans-Pacific transport of air pollutants. *Atmospheric Environment*, 37(3), 391– 404. https://doi.org/10.1016/S1352-2310(02)00862-2

Jardine, A. B., Jardine, K. J., Fuentes, J. D., Martin, S. T., Martins, G., Durgante, F., et al. (2015). Highly reactive light-dependent monoterpenes in the

Amazon. *Geophysical Research Letters*, 42, 1576– 1583. https://doi.org/10.1002/2014GL062573

Kavouras, I. G., Mihalopoulos, N., & Stephanou, E. G. (1998). Formation of atmospheric particles from organic acids produced by forests. *Nature*, 395(6703), 683– 686. https://doi.org/10.1038/27179

Kim, E., & Hopke, P. K. (2005). Improving source apportionment of fine particles in the eastern United States utilizing temperature-resolved carbon fractions. *Journal of the Air & Waste Management Association*, 55(10), 1456–1463. https://doi.org/10.1080/10473289.2005.10464748

Leaitch, W. R., Macdonald, A. M., Anlauf, K. G., Liu, P. S. K., Toom-Sauntry, D., Li, S.-M., et al. (2009). Evidence for Asian dust effects from aerosol plume measurements during INTEX-B 2006 near Whistler, BC. *Atmospheric Chemistry and Physics*, 9(11), 3523– 3546. https://doi.org/10.5194/acp-9-3523-2009

Liang, Q. (2005). Meteorological indices for Asian outflow and transpacific transport on daily to interannual timescales. *Journal of Geophysical Research*, 110, D18308. https://doi.org/10.1029/2005JD005788

Liang, Q., Jaeglé, L., Hudman, R. C., Turquety, S., Jacob, D. J., Avery, M. A., et al. (2007). Summertime influence of Asian pollution in the free troposphere over North America. *Journal of Geophysical Research*, 112, D12S11. https://doi.org/10.1029/2006JD007919

Lin, M., Fiore, A. M., Horowitz, L. W., Cooper, O. R., Naik, V., Holloway, J., et al. (2012). Transport of Asian ozone pollution into surface air over the western United States in spring: Asian influence on U.S. surface ozone. *Journal of Geophysical Research*, 117, D00V07. https://doi.org/10.1029/2011JD016961

Lin, M., Horowitz, L. W., Cooper, O. R., Tarasick, D., Conley, S., Iraci, L. T., et al. (2015). Revisiting the evidence of increasing springtime ozone mixing ratios in the free troposphere over western North America: Tropospheric ozone trends in Western NA. *Geophysical Research Letters*, 42, 8719– 8728. https://doi.org/10.1002/2015GL065311

Lin, M., Horowitz, L. W., Payton, R., Fiore, A. M., & Tonnesen, G. (2017). US surface ozone trends and extremes from 1980 to 2014: Quantifying the roles of rising Asian emissions, domestic controls, wildfires, and climate. *Atmospheric Chemistry and Physics*, 17(4), 2943– 2970. https://doi.org/10.5194/acp-17-2943-2017

Liu, J., Mauzerall, D. L., & Horowitz, L. W. (2009). Evaluating inter-continental transport of fine aerosols:(2) Global health impact. *Atmospheric Environment*, 43(28), 4339– 4347. https://doi.org/10.1016/j.atmosenv.2009.05.032

Martin, J. H., & Fitzwater, S. E. (1988). Iron-deficiency limits phytoplankton growth in the Northeast Pacific Subarctic. *Nature*, 331(6154), 341– 343. https://doi.org/10.1038/331341a0

McCoy, D. T., Burrows, S. M., Wood, R., Grosvenor, D. P., Elliott, S. M., Ma, P.-L., et al. (2015). Natural aerosols explain seasonal and spatial patterns of Southern Ocean cloud albedo. *Science Advances*, 1(6), e1500157. https://doi.org/10.1126/sciadv.1500157

McKendry, I. G., Macdonald, A. M., Leaitch, W. R., van Donkelaar, A., Zhang, Q., Duck, T., & Martin, R. V. (2008). Trans-Pacific dust events observed at Whistler, British Columbia during INTEX-B. *Atmospheric Chemistry and Physics*, 8(20), 6297– 6307. https://doi.org/10.5194/acp-8-6297-2008

Nastrom, G. D., & Gage, K. S. (1985). A climatology of atmospheric wavenumber spectra of wind and temperature observed by commercial aircraft. *Journal of the Atmospheric Sciences*, 42(9), 950– 960. https://doi.org/10.1175/1520-0469(1985)042%3C0950:ACOAWS%3E2.0.CO;2

Nriagu, J. O. (1990). The rise and fall of leaded gasoline. *Science of the Total Environment*, 92, 13– 28. https://doi.org/10.1016/0048-9697(90)90318-O

Paatero, P., Hopke, P. K., Song, X.-H., & Ramadan, Z. (2002). Understanding and controlling rotations in factor analytic models. *Chemometrics and Intelligent Laboratory Systems*, 60(1–2), 253– 264. https://doi.org/10.1016/S0169-7439(01)00200-3

Parrish, D. D., Law, K. S., Staehelin, J., Derwent, R., Cooper, O. R., Tanimoto, H., et al. (2012). Long-term changes in lower tropospheric baseline ozone concentrations at northern mid-latitudes. *Atmospheric Chemistry and Physics*, 12(23), 11,485– 11,504. https://doi.org/10.5194/acp-12-11485-2012

Pöschl, U. (2005). Atmospheric aerosols: Composition, transformation, climate and health effects. *Angewandte Chemie International Edition*, 44(46), 7520– 7540. https://doi.org/10.1002/anie.200501122

Rabbe, O. G., Braaten, D. A., Axelbaum, R. L., Teague, S. V., & Cahill, T. A. (1988). Calibration studies of the drum impactor. *Journal of Aerosol Science*, 19(2), 183– 195. https://doi.org/10.1016/0021-8502(88)90222-4

Rinne, H. J. I., Guenther, A. B., Greenberg, J. P., & Harley, P. C. (2002). Isoprene and monoterpene fluxes measured above Amazonian rainforest and their dependence on light and temperature. *Atmospheric Environment*, 36(14), 2421– 2426. https://doi.org/10.1016/S1352-2310(01)00523-4

Rosenfeld, D., Lohmann, U., Raga, G. B., O'Dowd, C. D., Kulmala, M., Fuzzi, S., et al. (2008). Flood or drought: How do aerosols affect precipitation? *Science*, 321(5894), 1309– 1313. https://doi.org/10.1126/science.1160606

Settle, D. M., & Patterson, C. C. (1982). Magnitudes and sources of precipitation and dry deposition fluxes of indestrial and natural leads to the

North Pacific at Enewetak. *Journal of Geophysical Research*, 87, 8857– 8869. https://doi.org/10.1029/JC087iC11p08857

Sindelarova, K., Granier, C., Bouarar, I., Guenther, A., Tilmes, S., Stavrakou, T., et al. (2014). Global data set of biogenic VOC emissions calculated by the MEGAN model over the last 30 years. *Atmospheric Chemistry and Physics*, 14(17), 9317– 9341. https://doi.org/10.5194/acp-14-9317-2014

Sun, Y., Zhang, Q., Macdonald, A. M., Hayden, K., Li, S. M., Liggio, J., et al. (2009). Size-resolved aerosol chemistry on Whistler Mountain, Canada with a high-resolution aerosol mass spectrometer during INTEX-B. *Atmospheric Chemistry and Physics*, 9(9), 3095– 3111. https://doi.org/10.5194/acp-9-3095-2009

Table of Historical Ozone National Ambient Air Quality Standards (NAAQS) (2018). Retrieved from https://www.epa.gov/ozone-pollution/table-historical-ozone-national-ambient-air-quality-standards-naaqs

Table of Historical Particulate Matter (PM) National Ambient Air Quality Standards (NAAQS) (2018). Retrieved August 25, 2017, from https://www.epa.gov/pm-pollution/table-historical-particulate-matter-pm-national-ambient-air-quality-standards-naaqs

Tan, M. G., Zhang, G. L., Li, X. L., Zhang, Y. X., Yue, W. S., Chen, J. M., et al. (2006). Comprehensive study of lead pollution in Shanghai by multiple techniques. *Analytical Chemistry*, 78(23), 8044– 8050. https://doi.org/10.1021/ac061365q

Uno, I., Eguchi, K., Yumimoto, K., Takemura, T., Shimizu, A., Uematsu, M., et al. (2009). Asian dust transported one full circuit around the globe. *Nature Geoscience*, 2(8), 557– 560. https://doi.org/10.1038/ngeo583

VanCuren, R. A. (2002). Asian aerosols in North America: Frequency and concentration of fine dust. *Journal of Geophysical Research*, 107(D24), 4804. https://doi.org/10.1029/2002JD002204

VanCuren, R. A. (2003). Asian aerosols in North America: Extracting the chemical composition and mass concentration of the Asian continental aerosol plume from long-term aerosol records in the western United States. *Journal of Geophysical Research*, 108(D20), 4623. https://doi.org/10.1029/2003JD003459

VanCuren, R. A., Cliff, S. S., Perry, K. D., & Jimenez-Cruz, M. (2005). Asian continental aerosol persistence above the marine boundary layer over the eastern North Pacific: Continuous aerosol measurements from Intercontinental Transport and Chemical Transformation 2002 (ITCT 2K2). *Journal of Geophysical Research*, 110, D09S90. https://doi.org/10.1029/2004JD004973

VanCuren, R. T., & Gustin, M. S. (2015). Identification of sources contributing to PM 2.5 and ozone at elevated sites in the western U.S. by receptor analysis: Lassen Volcanic National Park, California, and Great Basin National

Park, Nevada. *Science of the Total Environment*, 530-531, 505– 518. https://doi.org/10.1016/j.scitotenv.2015.03.091

Venecek, M. A., Zhao, Y., Mojica, J., McDade, C. E., Green, P. G., Kleeman, M. J., & Wexler, A. S. (2016). Characterization of the 8-stage Rotating Drum Impactor under low concentration conditions. *Journal of Aerosol Science*, 100, 140– 154. https://doi.org/10.1016/j.jaerosci.2016.07.007

Vernier, J.-P., Fairlie, T. D., Natarajan, M., Wienhold, F. G., Bian, J., Martinsson, B. G., et al. (2015). Increase in upper tropospheric and lower stratospheric aerosol levels and its potential connection with Asian pollution: ATAL nature and origin. *Journal of Geophysical Research: Atmospheres*, 120, 1608– 1619. https://doi.org/10.1002/2014JD022372

von der Weiden, S.-L., Drewnick, F., & Borrmann, S. (2009). Particle loss calculator—A new software tool for the assessment of the performance of aerosol inlet systems. *Atmospheric Measurement Techniques*, 2(2), 479–494. https://doi.org/10.5194/amt-2-479-2009

Went, F. W. (1960). Blue hazes in the atmosphere. *Nature*, 187(4738), 641–643. https://doi.org/10.1038/187641a0

Wexler, A. S., Green, P. G., Zhao, Y. J., Kleeman, M., McDade, C., & Venecek, M. (2015). RDI-MOUDI-IMPROVE intercomparison study (California Air Resources Board Project Report No. 12–309) (pp. 1–112). Air Quality Research Center: University of California-Davis.

World Health Organization (2013). Review of evidence on health aspects of air pollution—REVIHAAP project. Copenhagen:WHO Regional Office for Europe. Retrieved from http://www.euro.who.int/__data/assets/pdf_file/0004/193108/REVIHAAP-Final-technical-report-final-version.pdf?ua=1

Yu, H., Remer, L. A., Chin, M., Bian, H., Tan, Q., Yuan, T., & Zhang, Y. (2012). Aerosols from overseas rival domestic emissions over North America. *Science*, 337(6094), 566– 569. https://doi.org/10.1126/science.1217576

Zhao, T. L. (2003). Modeled size-segregated wet and dry deposition budgets of soil dust aerosol during ACE-Asia 2001: Implications for trans-Pacific transport. *Journal of Geophysical Research*, 108(D23), 8665. https://doi.org/10.1029/2002JD003363